Mechanobiology of Fibroblast Activation in Skin Grafting

Yuan Hong[1,2,*], Xiangjun Peng[1,3,*], Haomin Yu[1,2], Mohammad Jafari[1,4], Delaram Shakiba[1,5], Jacob Sandler[1,2], Kenneth M. Pryse[1,2], Elliot L. Elson[1,2,6], Guy M. Genin[1,2,3,#], Farid Alisafaei[1,4,#]

1. NSF Science and Technology Center for Engineering Mechanobiology
2. Department of Mechanical Engineering and Materials Science, Washington University in St. Louis
3. Department of Biomedical Engineering, Washington University in St. Louis
4. Department of Mechanical Engineering, New Jersey Institute of Technology
5. Department of Pathology, Saint Louis University School of Medicine
6. Department of Biochemistry and Molecular Biophysics, Washington University in St. Louis School of Medicine

Corresponding authors: farid.alisafaei@njit.edu, genin@wustl.edu
* These authors contributed equally to this work.

Abstract. Surgical repair of chronic wounds often requires split-thickness skin grafts in which epidermis and a thin part of the dermis from one site are harvested, cut into a meshwork, and stretched to cover a larger wound area. The main drawback of split-thickness skin grafting is excessive contracture of the skin graft in the wound site which is caused by the activation and transition of low-contractile fibroblasts to hyper-contractile myofibroblast cells. While a low amount of cellular contractile forces is required for wound healing, excessive contractile forces generated by hyperactivated cells can cause tightening of the skin graft, pain, scarring, and even graft failure. To test whether is a relationship between graft preparation and graft contracture, we hypothesized that the strain field that cells experience within a meshed graft regulates the activation of fibroblasts, and that the strain field and therefore cell activation level can be tailored by adjusting the meshing configurations to control the graft contracture. To test the hypothesis, we estimated strain fields of grafts with a wide range of clinically relevant meshing configurations, and evaluated the responses of human dermal fibroblasts to these strain levels within tissue constructs. We first showed that the choice of meshing configuration can induce a significant change in the graft strain level ranging from less than 5% to more than 30%. We then found that cells within tissue constructs statically stretched to 30% had significantly lower contractile force than cells within tissue constructs stretched to 5%. Data were used to fit a model of fibroblast activation, with activation peaking at a critical strain before decreasing due to cytoskeletal fluidization. The model was applied to predict conditions of meshing that tune graft contracture to desired levels. Results suggest a potential pathway for harnessing the memory of mechanical loading in fibroblasts to define and predict outcomes of skin graft surgeries.

Introduction

Many cells seemingly remember previous mechanical conditions through changes to gene or protein expression that persist over physiologically relevant timescales [1–3]. Much work in the field of mechanobiology points to mesenchymal stem cells remembering the stiffness of substrates to which they adhere through integrin ligation, affecting aspects of subsequent differentiation, and mesenchymal-derived cells such as myocytes strengthen or weaken depending upon past loading [4–8]. Specific agents of nuclear mechanotransduction have been identified, including molecules that can translocate to the nucleus under mechanical stress and affect subsequent gene expression in ways that are analogous to the transient storage of memory [9–14]. Wound healing and progression of fibrotic diseases involve mechanical changes in the extracellular environment of fibroblast cells including changes to mechanical strains felt by cells as well as changes to extracellular matrix (ECM) stiffness [15–17]. Although these changes are critical to outcomes in such settings, predictive models of the ways that fibroblasts store and respond to mechanical signals have not yet been extended to predict how mechanical stretch relates to subsequent fibroblast contractility in tissue settings. We therefore tested this in a tissue construct setting and used the data to verify and calibrate mathematical models of mechanical signal transduction and response in fibroblasts.

Smooth muscle cells and fibroblasts can exhibit more rapid changes to the cytoskeleton through the dynamics of actin and focal adhesion complexes. Actin polymerization occurs continuously within a cell, with actin fibers stabilized by focal adhesion complexes that receive sufficient loading to keep actin under a specific range of tension [18–23]. We hypothesized that reduction of tension below that range leads to increases in actin depolymerization rates, and exerting tension above that range leads to rapid fluidization of the actin cytoskeleton [23–27]. Thus, mild stretching of fibroblasts with a few percent would strengthen the cytoskeleton and increase the subsequent contractility of fibroblasts, while stretching sufficient to fluidize the cytoskeleton would insulate the nucleus from mechano-signaling [28] and therefore attenuate subsequent cell contractility. We hypothesized that this would have effects in the form of long-term activation or deactivation of fibroblasts. We tested this hypothesis by comparing contractility in tissue constructs stretched with 5% or 30%.

An area where this is particularly important is skin grafting surgeries. Each year only in America 8.2 million suffer a chronic wound arising from burns, diabetic ulcers, skin cancer surgery, or infection [29,30]. These fail to pass through the normal healing process and the body is not able to replace the damaged skin at the wound site [31–35]. To protect the wound from the environment and pathogens, larger chronic wounds are often treated with split-thickness skin grafts which consist of the epidermis and a thin part of the dermis taken from a donor or from one part of the body (Fig. 1A (i)), and then meshed with rows of small interrupted slits (Fig. 1A (ii)), stretched (Fig. 1A (iii)), and transplanted over a larger wound site (Fig. 1A (iv)) [36–39]. In the process of skin grafting and as a result of skin graft stretching, cells within the skin graft experience static tensile strains. We hypothesized that this stretching of a meshed skin graft would lead to spatial variations in strain associated with strain concentrations near the ends of slits, and tested this hypothesis using numerical simulations. With that hypothesis supported, we performed additional simulations based upon our experiments to establish the possibility of controlling future activation and contractility of fibroblasts and subsequently graft shrinkage by tuning spatial distributions of strain.

Results

The spatially varying strain fields experienced by cells in a skin graft can be controlled by changing the "meshing ratio". To test the hypothesis that the strain field within a graft varies with the meshing ratio, we evaluated how the strain field that cells experience in a skin graft is

affected by altering grafting parameters such as meshing ratio (Fig. 1B). Note that skin is not an isotropic material as it has orientation-dependent mechanical properties (Fig. 1C). This includes a critical effect of Langer's lines, also called cleavage lines, in different parts of the body. Langer's lines are topological lines that parallel the dominant orientation of collagen fibers and fibroblast cells in the dermis [40–45].

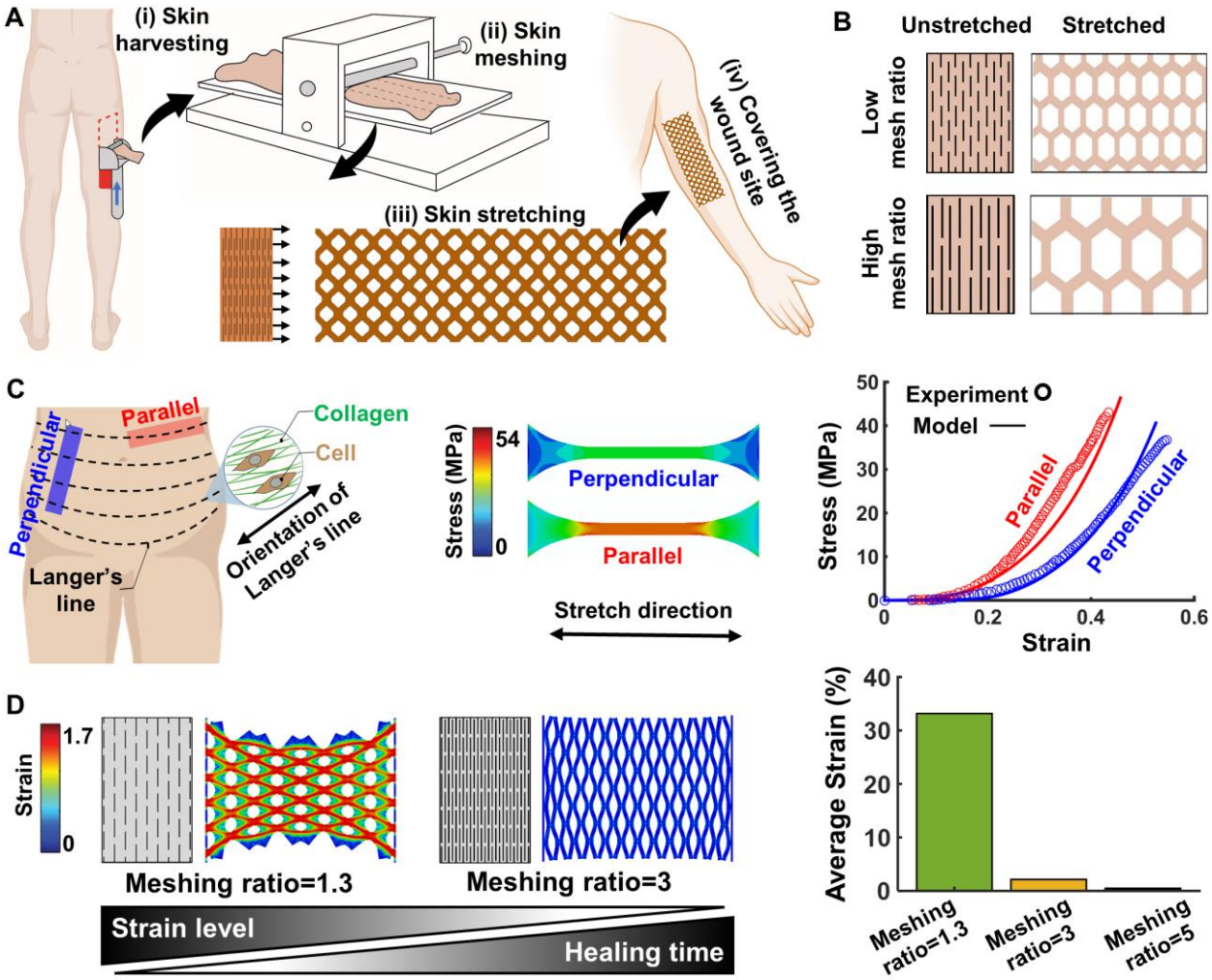

Figure 1. Skin graft meshing ratio can be tuned to tailor strain levels by an order of magnitude during graft stretching. (A) To protect from pathogens, large chronic wounds are often treated with split-thickness skin grafts in which epidermis and part of the dermis are harvested from a donor site (i), then cut into a meshwork of slits (ii) and stretched (iii) over a larger wound site (iv). (B) A skin graft can be meshed with different meshing ratios to cover a wound with a specific area. However, the choice of meshing ratio will impact the strain field that cells experience in the stretched skin graft. (C) To determine how the strain field in skin grafts changes with meshing ratio, we first calibrated a hyperelastic model against uniaxial stretching experiments of unmeshed skin grafts [46]. (D) We then used the calibrated model to determine how the strain field changes with meshing ratio. The simulations showed the strain fields experienced by cells depend strongly on the design of slits with the choice of meshing ratio affecting the average strains in graft tissue by an order of magnitude.

Skin grafts are harvested from the donor site in an orientation relative to the Langer's lines depending on the availability of the donor site and the wound size. For example, Fig. 1C shows skin grafts harvested from the donor site in two different orientations: perpendicular and parallel to the Langer's lines. As expected, mechanical testing of two such skin grafts shows that skin stretching in the direction of Langer's lines requires higher forces,[46] as collagen fibers are aligned in the direction of Langer's line and therefore the tissue exhibits higher stiffness in this direction (Fig. 1C) [47].

This anisotropic behavior of the skin can be approximated by a hyperelastic anisotropic continuum model [48,49] calibrated by fitting to skin stretching experiments, and implemented into a finite element framework (Fig. 1C). Using the calibrated skin model, we found that the strain distribution in stretched skin grafts depends strongly on the meshing ratio (Fig. 1D). Skin meshed with higher meshing ratios has higher numbers and longer cuts, and can be stretched easily without undergoing high tensile strains. These lower macroscopic strains mean that cells within skin grafts with higher meshing ratios experience lower strain levels [50]. Note that meshing ratios of 1 to 5 are frequently used in skin graft surgeries [51] and our results show that the choice of meshing ratio can induce more than an order of magnitude change in the average strain level that cells experience in the skin graft with average strains of over 30% possible (Fig. 1D).

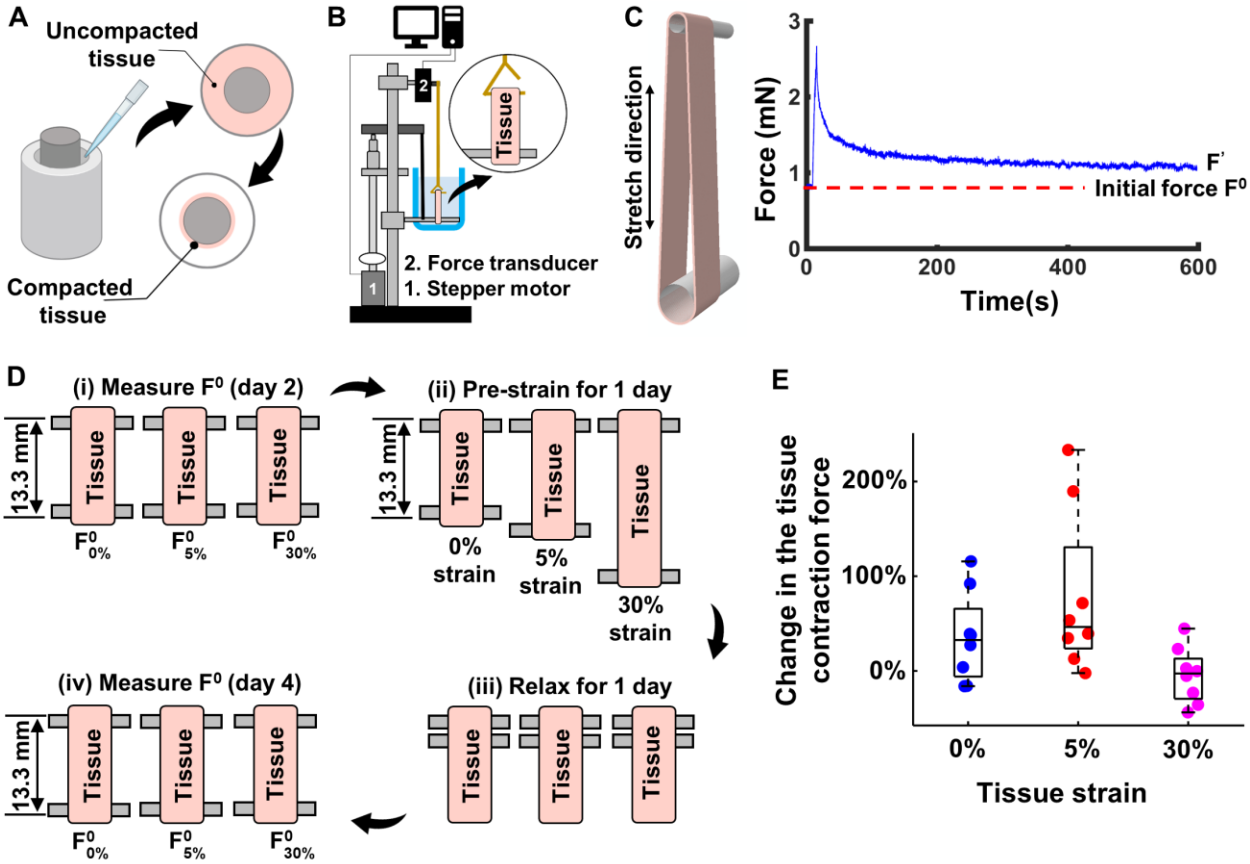

Figure 2. The strain field generated in stretched skin grafts determines the activation level of fibroblast cells. (A) To study how the strain field experienced by cells within stretched skin grafts affects cell activation level, we created thin tissues made of dermal fibroblast cells and type I collagen in a Teflon mold. The tissues were compacted over 2 days and formed thin contractile rings. (B) To measure the tissue contractility level, we used a custom-made tissue stretcher device with a temperature-controlled organ bath.

(C) A representative plot of tissue force measurements. The tissue contractility level was determined as the tissue contractile force F^0 measured upon hanging the tissue ring on the device. (D) To measure how the tissue strain field affects the tendency of tissues to contract, we first measured the tissue contractile force F^0 on day 2 (i). Based on the strain measurements of meshed skin grafts in Fig. 1D, we then statically exposed the tissues to 0, 5, and 30% strains for one day (ii), followed by releasing the load for one day (iii), and measurement of F^0. Note that all measurements of the tissue contractile force F^0 were done at a tissue length of 13.3 mm. At this length, the periphery of the tissues on the stretcher device is equal to the periphery of the tissues in the mold on day 2. (E) The change in the tissue contractile force [F^0(day 4) - F^0(day 2)] / F^0(day 2) demonstrated the long-term effect of the strain fields on the contractility level of the tissues.

Fibroblasts can be permanently activated or deactivated depending on the strain level that they experience in skin grafts. We next studied whether the 30 percent change in the strain level of cells can affect their behavior by inducing a long-term increase or decrease in cell contractility level. Note that both hyperactivation (an excessive increase of cell contractility) and deactivation (a significant decrease in cell contractility) of fibroblast cells in a skin graft can negatively affect the outcome of skin grafting. Thus, it is of crucial importance to determine optimal skin grafting strategies that prevent excessive contracture of skin grafts while keeping the baseline tissue contractility required for wound closure.

To measure how cell contractility changes with the strain level in skin grafts, we created thin layered tissues made of dermal fibroblast cells and type I collagen (Fig. 2A), and we used our custom-made tissue stretcher (Fig. 2B) [52] to measure the tissue contractile force F^0 (Fig. 2C). Note that in split-thickness skin grafts, the harvested skin graft is stretched to cover the wound area that is usually larger than the area of the original harvested skin, and more importantly, it remains stretched on the wound site for a few days until new skin is produced and tension decreased [53,54]. Therefore, to expose cells to a similar mechanical environment, we first measured the contractile force in our tissues after 2 days of tissue culturing (Fig. 2D (i)). We then statically exposed the tissues to different strain levels for one day (Fig. 2D (ii)), followed by releasing the load and allowing the tissues to relax for one day (Fig. 2D (iii)). Finally, we measured the contractile force in the tissues again (Fig. 2D (iv)) to determine whether being exposed to tensile strains has induced a permanent change in their contractility levels.

Our results showed that the contractility level of cells and the traction force they generate depend on the magnitude of strain that they experience in their skin graft (Fig. 2E); tissue stretching even with a small strain of 5% drove cells permanently into a higher contractile state, while very large strains significantly reduced tissue contractile force. This indicates that the level of strain that cells experience in skin grafts can affect the outcome of skin graft surgeries as hypercontractility of cells can cause excessive tissue contraction, while low contractility of cells can delay and even curtail the wound healing process.

The increase and decrease in tissue contraction levels are associated with activation and deactivation of cells and not changes in the mechanical properties of the extracellular environment. To ensure that the observed increase and decrease in tissue contraction levels are associated with changes in the contractility of individual cells and not changes in the physical properties of the tissues, we decoupled the effects of cells and matrix using our previously developed approach [52]. In non-muscle cells, the cellular forces are generated by the actomyosin machinery [55,56]. The myosin head domains bind to actin filaments and pull on them to generate internal contractile forces which are transmitted to the extracellular matrix [57,58], and produce the total tissue contractile force F^0 (Fig. 2C). Thus, changes in the contractility level of individual cells

or in the physical properties of the extracellular collagen matrix can affect the total tissue contractile force F^0.

To decouple the effects of cells and matrix on the total tissue contractile force F^0, we first measured the responses of the tissues (containing cells and matrix) under a tensile relaxation test (Fig. 3A (ii)). We then treated the tissues with cytochalasin-D to disrupt the actomyosin contractility of the cells (Fig. 3A (iii)). Finally, we tested the cytochalasin-D treated tissues with the same relaxation test to determine the responses of the collagen matrices (Fig. 3A (iv)). The disruption of actomyosin contractility in cytochalasin-D treated tissues can be seen in Fig. 3B where, unlike untreated tissues, they do not exhibit tissue contraction ($F^0 \sim 0$) and therefore the relaxation test shows only the passive properties of the tissues.

Our results showed that the tissues with 0, 5, and 30% pre-strain levels all exhibited the same response to the relaxation test after cytochalasin-D treatment. This is shown in Fig. 3C where all cytochalasin-D treated tissues have the same stiffness (passive stiffness). This indicates that the collagen matrices in the tissues have the same physical properties and therefore the biphasic change in the tissue contraction in Fig. 2E is due to changes in cell contractility and is not associated with changes in collagen properties.

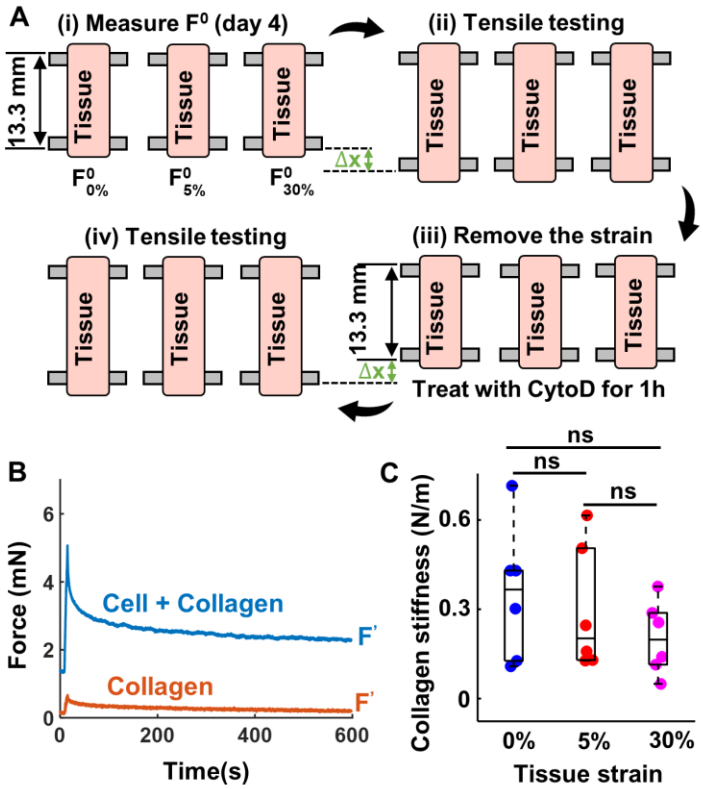

Figure 3. The long-term effect of pre-straining on tissue contractility is due to activation/deactivation of fibroblasts and not damage to the extracellular matrix. (A) The physical properties of tissues were determined using a relaxation test before (ii) and after (iv) disruption of cell actomyosin contractility. (B) A representative plot of tissue response to the relaxation test before (blue line) and after (orange line) disruption of cell actomyosin contractility. (C) Tissue stiffness (F'/Δx) after disruption of cell actomyosin contractility exhibited no change with pre-strain level, indicating that the changes in tissue contractility in Fig. 2E are not due to changes in collagen properties.

A bio-chemo-mechanical model to relate cellular activation and deactivation to mechanical memory of cells as a function of magnitude and duration of skin graft stretching. To understand the mechanism through which skin graft stretching causes the biphasic trend in cell actomyosin contractility in Fig. 2E and building upon our previous work [59], we developed a bio-chemo-mechanical model that accounts for the key cellular components involved in the generation and transmission of cellular contractile forces (Fig. 4A). We first describe the components of the active model and validate the model predictions without the presence of external forces. We then show how the model responds to external forces caused by skin graft stretching.

The first element of the cell model is myosin motors which generate cell internal contractility as we have previously shown in our experiments [60]. The force generated by myosin σ_{myosin} causes compressive stress $E_{\mathrm{MT}}\,\varepsilon_{\mathrm{MT}}$ and tensile stress σ in the cytoskeletal components that are in compression (e.g., microtubules) and tension (e.g., actin elements), respectively,

$$\sigma_{\mathrm{myosin}} = -E_{\mathrm{MT}}\,\varepsilon_{\mathrm{MT}} + \sigma \tag{1}$$

where E_{MT} and $\varepsilon_{\mathrm{MT}}$ are the stiffness and strain of the cytoskeletal components that are in compression, and σ denotes the tensile stress in the cytoskeletal components that are in tension (e.g., actin elements) which is also the total cell traction stress transmitted to the extracellular matrix (Fig. 4A). The second element of the model is microtubules, which are connected to the contractile element in parallel and subsequently experience compression in agreement with experimental reports (Fig. 4A) [61,62]. The third element of the model is actin filaments which are connected to the myosin element in series (Fig. 4A). Thus, the actin element experiences tension and transmits the myosin-generated tensile force σ_{myosin} to the extracellular matrix as reported experimentally [63–65]. We and others have shown that cells respond to tension (generated either by the intrinsic cell contractility or external tensile forces) by recruiting and alignment of actin filaments in the direction of tension [65–67,27,59,23]. However, increasing tension on actin filaments beyond a threshold can lead to depolymerization of actin filaments and cell fluidization (Figs. 4B-4C) [23]. To include the polymerization and depolymerization of actin filaments in our model, the stiffness of the actin element, denoted by the slop of the stress-strain curve in Fig. 4B, initially increases with tension representing actin polymerization followed by damage and fluidization of the actin element.

We next validated the model responses to chemo-mechanical signals before studying how the model responds to stretching. We first simulated disruption of the microtubule and actin networks by decreasing the stiffness of the microtubule and actin elements, E_{MT} and E_{actin}, respectively (Fig. 4E). We have previously shown that depolymerization of microtubules increases cell contractility through activation of the Rho-Rock pathway [56]. In agreement with these experiments, our simulations showed that phosphorylation of myosin motors and subsequently the force generated by myosin σ_{myosin} as well as the cell traction stress σ increased with decreasing microtubule stiffness. These simulations were also validated by our experiments which showed that dermal fibroblasts within a 3D fibrous environment became more contractile with depolymerization of microtubules upon nocodazole treatment, and subsequently generated higher forces and stretched the matrix more (Fig. 4D), which were all consistent with other experimental measurements [68–71]. Furthermore, the model showed that depolymerization of actin filaments reduced myosin phosphorylation and cell traction stress (Fig. 4E) which was in agreement with our experiments where disruption of actin upon cytochalasin-D treatment decreased cell traction forces and subsequently collagen accumulation (Fig. 4D) [72]. We next validated the model responses to matrix stiffness by simulating cell responses to micro-pillar stiffness [65]. Our simulations showed that both phosphorylation of myosin motors and cell traction force monotonically increased with micro-pillar stiffness and then reached a plateau (Fig. 4F) in

agreement with experimental studies of fibroblast cells cultured on micro-pillars with different stiffness [65].

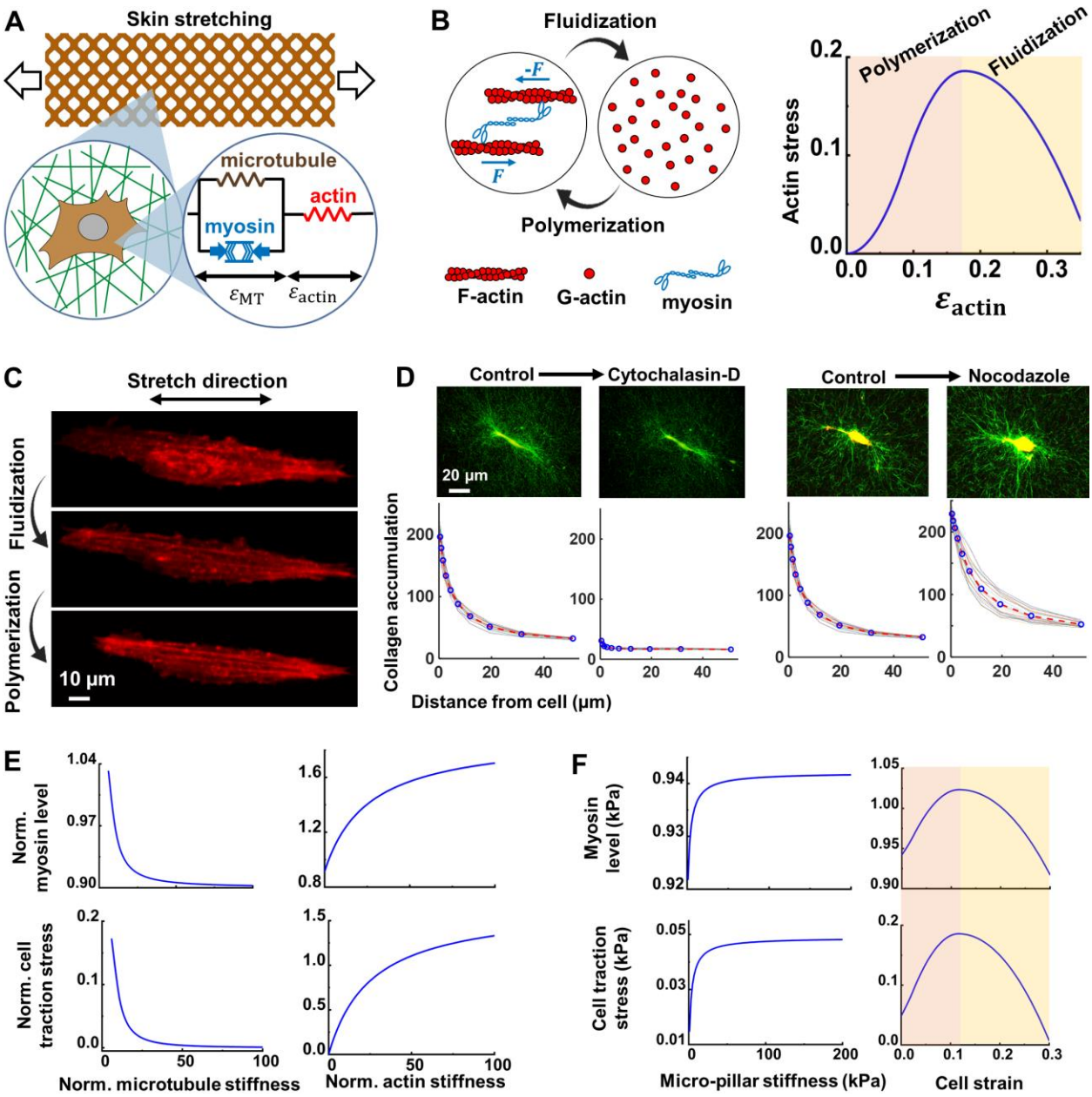

Figure 4. Mathematical modeling of cell activation/deactivation in skin grafting. (A) The cell is modeled as a continuum of representative volume elements (RVEs), each of which is constructed by connecting the key cellular components involved in the generation and transmission of cellular forces, including (i) an active force-generating contractile element representing myosin motors, (ii) the microtubule network, and (iii) the actin filament network. (B) Response of the actin element in the model to tension. (C) Stretching of fibroblasts can cause both depolymerization and polymerization of actin filaments along the stretch direction. (D) Disruption of actomyosin and microtubule networks decreased and increased cellular contractile force and subsequently collagen accumulation, respectively. (E) In agreement with the experiments, the model showed that reduction of the stiffness of the actin and microtubule networks decreased and increased myosin phosphorylation and cell traction force, respectively. (F) Unlike cell

response to stiffening of the extracellular matrix where myosin phosphorylation and cell traction force monotonically increased and then reached a plateau, the cell model exhibited a significant drop in cell force generation at high strains consistent with our experimental measurements in Fig.2E.

After validating the model responses to chemical treatments and matrix stiffening, we tested the model under the external tensile strains ranging from 0 to about 30 percent as measured in our stretched skin grafts (Fig. 1D). Our simulations showed that, unlike the monotonic cell responses to matrix stiffening, both myosin phosphorylation and cell traction force exhibited a biphasic behavior with cell strain (Fig. 4F); for small strains, cell actomyosin contractility increased with cell strain, while stretching of the cell beyond a strain threshold caused cell fluidization and significant reduction of actomyosin contractility. These simulations are in agreement with our experiments in Fig. 2E where increasing cell strain from 5 to 30 percent permanently transformed hypercontractile fibroblasts into deactivated cells.

Conclusions

Cells in skin grafts undergo stresses whose magnitude and orientation depend on surgical parameters including meshing ratio, meshing orientation, skin physical properties, and wound site geometry. While current grafting protocols do not account for these mechanobiological factors, our results showed that these stresses and their durations can activate nuclear mechanosensing pathways and drive fibroblast cells to a higher or lower contractile phenotype. Using an integrated experimental and theoretical approach, we showed that by tailoring of meshing configuration, we can harness the molecular machinery of mechanotransduction to enable skin graft contracture that prevents excessive contracture while keeping the baseline contractility required for wound closure.

Material and methods

Tensile stretcher

The custom-made tensile tester with sensitive isometric force transducers (Harvard Apparatus) and stepper motors (Haward Industry) was plugged into an Arduino for applying displacement precisely. A MATLAB code was developed for collecting the output voltages reported by these transducers, which were calibrated to the force. To control the temperature, a water pump with a temperature control system was connected to the organ bath (Fig. 2B).

Cell culture and tissue construction

Human dermal fibroblasts (HDFs, Lonza) were maintained with Dulbecco's Modified Eagle Medium (DMEM, Gibco) supplemented with 10% fetal bovine serum (FBS, Gibco) and 1% penicillin-streptomycin (PS, Gibco). The HDFs were trypsinized, resuspended in fresh DMEM and then added to mouse rat tail-derived type I collagen in 0.1% acetic acid and 2X DMEM (Sigma). After neutralizing the pH with 1 M sodium hydroxide, 1 mL of the mixture containing 1.5×10^6 cells/mL HDFs and 1.2 mg/mL collagen was poured into each cylindrical casting well and was incubated at 37 °C with 5% CO_2 for 2 days for the polymerization and compaction of the tissue.

These casting wells for tissue construction were made with Teflon and have a mandrel with a diameter of 9.652 mm at the center to construct a tissue ring for the tensile test (Fig. 2A).

The tissue rings were removed from the casting wells and hung onto the attachment bars, bathed with 25 mM HEPES buffered DMEM with 10% FBS and 1% PS at 37 °C. Then the attachment bars were separated at a 13.3 mm distance under the control of the Arduino. The initial force was measured by lifting the lower attachment bars away from the samples to define the zero-force points. The samples were moved to a pre-strain setup in sodium bicarbonate buffered DMEM at 37 °C with 5% CO_2 for desired strain levels with 3D printed spacers with different lengths for 1d. Then the spacers were removed to relax the tissues for another day. After repeating the initial force measurements, 5% strain was applied to the samples through Arduino for 10 mins (Fig. 3A). Then, the samples were relaxed for 10 mins before being treated with 2 micromolar (µM) cytochalasin-D (Sigma) for 1h. The cytochalasin-D treated samples were again tested with the 5% strain for 10 mins (Fig. 3A).

References

1. Li, C. X. *et al.* MicroRNA-21 preserves the fibrotic mechanical memory of mesenchymal stem cells. *Nat. Mater.* **16**, 379–389 (2017).
2. Balestrini, J. L., Chaudhry, S., Sarrazy, V., Koehler, A. & Hinz, B. The mechanical memory of lung myofibroblasts. *Integr. Biol.* **4**, 410–421 (2012).
3. Yang, C., Tibbitt, M. W., Basta, L. & Anseth, K. S. Mechanical memory and dosing influence stem cell fate. *Nat. Mater.* **13**, 645–652 (2014).
4. Engler, A. J., Sen, S., Sweeney, H. L. & Discher, D. E. Matrix Elasticity Directs Stem Cell Lineage Specification. *Cell* **126**, 677–689 (2006).
5. Bian, L., Guvendiren, M., Mauck, R. L. & Burdick, J. A. Hydrogels that mimic developmentally relevant matrix and N-cadherin interactions enhance MSC chondrogenesis. *Proc. Natl. Acad. Sci.* **110**, 10117–10122 (2013).
6. Zhang, C. *et al.* Mechanics-driven nuclear localization of YAP can be reversed by N-cadherin ligation in mesenchymal stem cells. *Nat. Commun.* **12**, 6229 (2021).
7. Mondrinos, M. J. *et al.* Surface-directed engineering of tissue anisotropy in microphysiological models of musculoskeletal tissue. *Sci. Adv.* **7**, eabe9446 (2021).
8. Killaars, A. R. *et al.* Extended Exposure to Stiff Microenvironments Leads to Persistent Chromatin Remodeling in Human Mesenchymal Stem Cells. *Adv. Sci.* **6**, 1801483 (2019).
9. Dupont, S. & Wickström, S. A. Mechanical regulation of chromatin and transcription. *Nat. Rev. Genet.* **23**, 624–643 (2022).
10. Elosegui-Artola, A. *et al.* Force Triggers YAP Nuclear Entry by Regulating Transport across Nuclear Pores. *Cell* **171**, 1397-1410.e14 (2017).
11. Andreu, I. *et al.* The force loading rate drives cell mechanosensing through both reinforcement and cytoskeletal softening. *Nat. Commun.* **12**, 4229 (2021).
12. Nasrollahi, S. *et al.* Past matrix stiffness primes epithelial cells and regulates their future collective migration through a mechanical memory. *Biomaterials* **146**, 146–155 (2017).
13. Price, C. C., Mathur, J., Boerckel, J. D., Pathak, A. & Shenoy, V. B. Dynamic self-reinforcement of gene expression determines acquisition of cellular mechanical memory. *Biophys. J.* **120**, 5074–5089 (2021).
14. Niu, L. *et al.* A positive mechanobiological feedback loop controls bistable switching of cardiac fibroblast phenotype. *Cell Discov.* **8**, 1–16 (2022).
15. Tschumperlin, D. J., Ligresti, G., Hilscher, M. B. & Shah, V. H. Mechanosensing and fibrosis. *J. Clin. Invest.* **128**, 74–84 (2018).
16. Hinz, B. Formation and Function of the Myofibroblast during Tissue Repair. *J. Invest. Dermatol.* **127**, 526–537 (2007).
17. Alisafaei, F., Chen, X., Leahy, T., Janmey, P. A. & Shenoy, V. B. Long-range mechanical signaling in biological systems. *Soft Matter* **17**, 241–253 (2021).

18. Elson, E. L. & Genin, G. M. The role of mechanics in actin stress fiber kinetics. *Exp. Cell Res.* **319**, 2490–2500 (2013).
19. Kaunas, R. & Hsu, H.-J. A kinematic model of stretch-induced stress fiber turnover and reorientation. *J. Theor. Biol.* **257**, 320–330 (2009).
20. Hsu, H.-J., Lee, C.-F. & Kaunas, R. A Dynamic Stochastic Model of Frequency-Dependent Stress Fiber Alignment Induced by Cyclic Stretch. *PLOS ONE* **4**, e4853 (2009).
21. Reynolds, N. H., McEvoy, E., Panadero Pérez, J. A., Coleman, R. J. & McGarry, J. P. Influence of multi-axial dynamic constraint on cell alignment and contractility in engineered tissues. *J. Mech. Behav. Biomed. Mater.* **112**, 104024 (2020).
22. McGarry, J. P. *et al.* Simulation of the contractile response of cells on an array of micro-posts. *Philos. Trans. R. Soc. Math. Phys. Eng. Sci.* **367**, 3477–3497 (2009).
23. Lee, S.-L. *et al.* Physically-Induced Cytoskeleton Remodeling of Cells in Three-Dimensional Culture. *PLoS ONE* **7**, e45512 (2012).
24. Trepat, X. *et al.* Universal physical responses to stretch in the living cell. *Nature* **447**, 592–595 (2007).
25. Lan, B. *et al.* Transient stretch induces cytoskeletal fluidization through the severing action of cofilin. *Am. J. Physiol.-Lung Cell. Mol. Physiol.* **314**, L799–L807 (2018).
26. Nekouzadeh, A., Pryse, K. M., Elson, E. L. & Genin, G. M. Stretch-activated force shedding, force recovery, and cytoskeletal remodeling in contractile fibroblasts. *J. Biomech.* **41**, 2964–2971 (2008).
27. Icard-Arcizet, D., Cardoso, O., Richert, A. & Hénon, S. Cell stiffening in response to external stress is correlated to actin recruitment. *Biophys. J.* **94**, 2906–2913 (2008).
28. Heterochromatin-Driven Nuclear Softening Protects the Genome against Mechanical Stress-Induced Damage. *Cell* **181**, 800-817.e22 (2020).
29. Sen, C. K. Human Wounds and Its Burden: An Updated Compendium of Estimates. *Adv. Wound Care* **8**, 39–48 (2019).
30. Sen, C. K. Human Wound and Its Burden: Updated 2020 Compendium of Estimates. *Adv. Wound Care* **10**, 281–292 (2021).
31. Frykberg, R. G. & Banks, J. Challenges in the Treatment of Chronic Wounds. *Adv. Wound Care* **4**, 560–582 (2015).
32. Siddiqui, A. R. & Bernstein, J. M. Chronic wound infection: Facts and controversies. *Clin. Dermatol.* **28**, 519–526 (2010).
33. Han, G. & Ceilley, R. Chronic Wound Healing: A Review of Current Management and Treatments. *Adv. Ther.* **34**, 599–610 (2017).
34. Powers, J. G., Higham, C., Broussard, K. & Phillips, T. J. Wound healing and treating wounds: Chronic wound care and management. *J. Am. Acad. Dermatol.* **74**, 607–625 (2016).
35. Li, M., Liang, Y., He, J., Zhang, H. & Guo, B. Two-Pronged Strategy of Biomechanically Active and Biochemically Multifunctional Hydrogel Wound Dressing To Accelerate Wound Closure and Wound Healing. *Chem. Mater.* **32**, 9937–9953 (2020).
36. Andreassi, A., Bilenchi, R., Biagioli, M. & D'Aniello, C. Classification and pathophysiology of skin grafts. *Clin. Dermatol.* **23**, 332–337 (2005).
37. Chuenkongkaew, T. Modification of Split-Thickness Skin Graft: Cosmetic Donor Site and Better Recipient Site. *Ann. Plast. Surg.* **50**, 212–214 (2003).
38. Lagus, H., Sarlomo-Rikala, M., Böhling, T. & Vuola, J. Prospective study on burns treated with Integra®, a cellulose sponge and split thickness skin graft: Comparative clinical and histological study—Randomized controlled trial. *Burns* **39**, 1577–1587 (2013).
39. Ayaz, M., Najafi, A. & Karami, M. Y. Thin Split Thickness Skin Grafting on Human Acellular Dermal Matrix Scaffold for the Treatment of Deep Burn Wounds. *Int. J. Organ Transplant. Med.* **12**, 44–51 (2021).
40. Ní Annaidh, A., Bruyère, K., Destrade, M., Gilchrist, M. D. & Otténio, M. Characterization of the anisotropic mechanical properties of excised human skin. *J. Mech. Behav. Biomed. Mater.* **5**, 139–148 (2012).
41. Gibson, T. Karl Langer (1819–1887) and his lines. *Br. J. Plast. Surg.* **31**, 1–2 (1978).
42. Carmichael, S. W. The tangled web of Langer's lines. *Clin. Anat.* **27**, 162–168 (2014).
43. Langer, K. On the anatomy and physiology of the skin: I. The cleavability of the cutis. *Br. J. Plast. Surg.* **31**, 3–8 (1978).
44. Bush, M. A., Thorsrud, K., Miller, R. G., Dorion, R. B. J. & Bush, P. J. The Response of Skin to Applied Stress: Investigation of Bitemark Distortion in a Cadaver Model*. *J. Forensic Sci.* **55**, 71–76 (2010).

45. Bush, J., Ferguson, M. W. J., Mason, T. & McGrouther, G. The dynamic rotation of Langer's lines on facial expression. *J. Plast. Reconstr. Aesthet. Surg.* **60**, 393–399 (2007).
46. Ní Annaidh, A. *et al.* Automated Estimation of Collagen Fibre Dispersion in the Dermis and its Contribution to the Anisotropic Behaviour of Skin. *Ann. Biomed. Eng.* **40**, 1666–1678 (2012).
47. Capek, L., Flynn, C., Molitor, M., Chong, S. & Henys, P. Graft orientation influences meshing ratio. *Burns* **44**, 1439–1445 (2018).
48. Gasser, T. C., Ogden, R. W. & Holzapfel, G. A. Hyperelastic modelling of arterial layers with distributed collagen fibre orientations. *J. R. Soc. Interface* **3**, 15–35 (2006).
49. Holzapfel, G. A., Gasser, T. C. & Ogden, R. W. A New Constitutive Framework for Arterial Wall Mechanics and a Comparative Study of Material Models. *J. Elast. Phys. Sci. Solids* **61**, 1–48 (2000).
50. Marquez, J. P., Elson, E. L. & Genin, G. M. Whole cell mechanics of contractile fibroblasts: relations between effective cellular and extracellular matrix moduli. *Philos. Trans. R. Soc. Math. Phys. Eng. Sci.* **368**, 635–654 (2010).
51. Kan, T. *et al.* Calculation of practical skin donor area for meshed skin grafting in real-world surgery. *Dermatol. Ther.* **33**, e14393 (2020).
52. Wakatsuki, T., Kolodney, M. S., Zahalak, G. I. & Elson, E. L. Cell Mechanics Studied by a Reconstituted Model Tissue. *Biophys. J.* **79**, 2353–2368 (2000).
53. Darcy, C. M. A technique for preparing meshed skin grafts with planned expansion ratios. *Br. J. Plast. Surg.* **56**, 77–79 (2003).
54. Zöllner, A. M., Holland, M. A., Honda, K. S., Gosain, A. K. & Kuhl, E. Growth on demand: Reviewing the mechanobiology of stretched skin. *J. Mech. Behav. Biomed. Mater.* **28**, 495–509 (2013).
55. Wakatsuki, T., Schwab, B., Thompson, N. C. & Elson, E. L. Effects of cytochalasin D and latrunculin B on mechanical properties of cells. *J. Cell Sci.* **114**, 1025–1036 (2001).
56. Kolodney, M. S. & Elson, E. L. Contraction due to microtubule disruption is associated with increased phosphorylation of myosin regulatory light chain. *Proc. Natl. Acad. Sci.* **92**, 10252–10256 (1995).
57. Pollard, T. D. Structure and polymerization of Acanthamoeba myosin-II filaments. *J. Cell Biol.* **95**, 816–825 (1982).
58. Shenoy, V. B., Wang, H. & Wang, X. A chemo-mechanical free-energy-based approach to model durotaxis and extracellular stiffness-dependent contraction and polarization of cells. *Interface Focus* **6**, 20150067 (2016).
59. Alisafaei, F., Jokhun, D. S., Shivashankar, G. V. & Shenoy, V. B. Regulation of nuclear architecture, mechanics, and nucleocytoplasmic shuttling of epigenetic factors by cell geometric constraints. *Proc. Natl. Acad. Sci.* **116**, 13200–13209 (2019).
60. Kolodney, M. S. & Elson, E. L. Correlation of myosin light chain phosphorylation with isometric contraction of fibroblasts. *J. Biol. Chem.* **268**, 23850–23855 (1993).
61. Wang, N. *et al.* Mechanical behavior in living cells consistent with the tensegrity model. *Proc. Natl. Acad. Sci.* **98**, 7765–7770 (2001).
62. Stamenović, D., Mijailovich, S. M., Tolić-Nørrelykke, I. M., Chen, J. & Wang, N. Cell prestress. II. Contribution of microtubules. *Am. J. Physiol.-Cell Physiol.* **282**, C617–C624 (2002).
63. Katoh, K., Kano, Y., Masuda, M., Onishi, H. & Fujiwara, K. Isolation and Contraction of the Stress Fiber. *Mol. Biol. Cell* **9**, 1919–1938 (1998).
64. Kumar, S. *et al.* Viscoelastic Retraction of Single Living Stress Fibers and Its Impact on Cell Shape, Cytoskeletal Organization, and Extracellular Matrix Mechanics. *Biophys. J.* **90**, 3762–3773 (2006).
65. Ghibaudo, M. *et al.* Traction forces and rigidity sensing regulate cell functions. *Soft Matter* **4**, 1836 (2008).
66. Oakes, P. W., Banerjee, S., Marchetti, M. C. & Gardel, M. L. Geometry Regulates Traction Stresses in Adherent Cells. *Biophys. J.* **107**, 825–833 (2014).
67. Hall, M. S. *et al.* Fibrous nonlinear elasticity enables positive mechanical feedback between cells and ECMs. *Proc. Natl. Acad. Sci.* **113**, 14043–14048 (2016).
68. Rape, A., Guo, W. & Wang, Y. Microtubule depolymerization induces traction force increase through two distinct pathways. *J. Cell Sci.* **124**, 4233–4240 (2011).
69. Danowski, B. A. Fibroblast contractility and actin organization are stimulated by microtubule inhibitors. *J. Cell Sci.* **93**, 255–266 (1989).
70. Chrzanowska-Wodnicka, M. & Burridge, K. Rho-stimulated contractility drives the formation of stress fibers and focal adhesions. *J. Cell Biol.* **133**, 1403–1415 (1996).

71. Kim, A. & Matthew Petroll, W. Microtubule regulation of corneal fibroblast morphology and mechanical activity in 3-D culture. *Exp. Eye Res.* **85**, 546–556 (2007).
72. Shakiba, D. *et al.* The Balance between Actomyosin Contractility and Microtubule Polymerization Regulates Hierarchical Protrusions That Govern Efficient Fibroblast–Collagen Interactions. *ACS Nano* **14**, 7868–7879 (2020).